# Six-phase Fractional-slot Concentrated Winding Ferrite Spoke-type Permanent Magnet Synchronous Motor for Electric Truck


Hoyun Won
Department of Electrical and Computer Engineering
The University of Alabama
Tuscaloosa, AL, USA
hwon@crimson.ua.edu

Yang-Ki Hong
Department of Electrical and Computer Engineering
The University of Alabama
Tuscaloosa, AL, USA
ykhong@eng.ua.edu

Jonathan Platt
Department of Electrical and Computer Engineering
The University of Alabama
Tuscaloosa, AL, USA
jtplatt@crimson.ua.edu

Minyeong Choi
Department of Electrical and Computer Engineering
The University of Alabama
Tuscaloosa, AL, USA
mchoi11@crimson.ua.edu

Briana Bryant
Department of Electrical and Computer Engineering
The University of Alabama
Tuscaloosa, AL, USA
bmbryant1@crimson.ua.edu

Seungdeog Choi
Department of Electrical Engineering
Mississippi State University
Starkville, MS, USA
seungdeog@ece.msstate.edu



***Abstract*— This paper presents a novel stator-shifted six-phase fractional-slot concentrated winding ferrite spoke-type permanent magnet synchronous machine for an electric truck application. The proposed motor consists of a stator with dual three-phase windings that are 75 degrees apart and a rotor with a ferrite permanent magnet in spoke configuration. To further reduce the torque ripple, one circular void and notch are introduced on the stator and rotor, respectively. The simulation results show that the proposed motor exhibits 138% lower torque ripple, 108 % lower back-EMF at 3000 rpm, and 95.5 % higher maximum speed with a maximum torque of 2150 Nm and no demagnetization, compared to three-phase integrated-slot distributed winding NdFeB V-type PMSM of Prius 2010.**



***Keywords*— *Ferrite permanent magnet motor, spoke-type configuration, stator-shift, six-phase, electric truck***


## I. Introduction

Electric vehicles and trucks have received much attention due to their ability to reduce $CO_2$ emissions and gasoline consumption and recent social infrastructure change caused by the COVID-19. Accordingly, the number of electric cars and trucks will increase respectively from 3,268,671 to 26,951,318 and from 60,000 to 350,000 in the next 10 years [1,2]. In electric vehicles, three-phase integrated slot distributed winding (ISDW) rare-earth-based NdFeB permanent magnet synchronous motors (PMSM) are widely adopted due to their high torque density, efficiency, and maximum speed. However, such a motor is not suitable for electric truck applications due to the following drawbacks [3,4]. First, despite three-phase motors offering the most cost-effective performance compared to other multi-phase motors, they suffer from high induced voltage and fault-intolerant operation [5]. Among winding configurations, ISDW is generally selected due to offering high saliency, which increases the maximum speed and power via the flux weakening. However, ISDW has disadvantages such as a long end winding, low-slot fill factor, and high torque ripple [5]. Lastly, although the rare-earth NdFeB permanent magnet (PM) offers good motor performance, its high cost, unstable rare-earth supply chain, and low resistance present challenges [5].

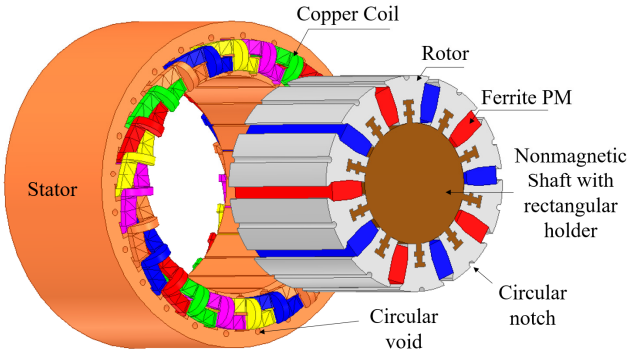


Fig. 1. Design of proposed six-phase stator-shifted fractional slot concentrated winding ferrite spoke-type permanent magnet synchronous motor (6Φ-S-FSCW-FSPMSM).

In this paper, we present a new six-phase stator-shifted fractional slot concentrated winding ferrite spoke-type PMSM (6Φ-S-FSCW-FSPMSM). Figure 1 shows the 3D-design of the proposed 6Φ-S-FSCW-FSPMSM. Table I summarizes the proposed motor specifications. The 6Φ-S-FSCW-FSPMSM consists of (i) a stator with a dual three-phase winding that has a mechanical phase shift of 75 degrees between two three-phase windings, (ii) a rotor in the spoke configuration, (iii) ferrite PMs (Hitachi: NMF-12F) with a remanent flux density of 0.45 T and coercivity of 329 kA/m at room temperature, (iv) one circular


This work was supported in part by National Science Foundation IUCRC under Grant number IPP-1650564.

TABLE I. SPECIFICATIONS OF PROPOSED 6Φ-S-FSCW-FSPMSM.

| Parameter | Value |
|---|---|
| Stator Outer/inner diameter [mm] | 525/351 |
| Rotor Outer/inner diameter [mm] | 348/196 |
| Stack Length [mm] | 270 |
| Number of slot/pole | 24/10 |
| Number of turns | 32 |
| Number of parallel paths | 8 |
| Maximum current [$A_{rms}$] | 500 |
| Peak power density [Nm/L] | 37.0 |
| Soft Iron Core Material | M19-29G |
| Base/Maximum speed [rpm] | 2400/4950 |

TABLE II. PERFORMANCE COMPARISON BETWEEN FOUR TOPOLOGIES.

| Parameter | SPM | PMASynRM | V-type | Spoke-type |
|---|---|---|---|---|
| Torque [Nm] | 1670 | 1710 | 1250 | 1880 |
| Torque Ripple [%] | 3.6 | 10.4 | 14.5 | 12.2 |
| Peak Back EMF at 3000 rpm [V] | 1200 | 2888 | 3023 | 2428 |

hole on the stator and notch on the rotor, and (v) a nonmagnetic shaft with a rectangular holder to rotate the rotor. This proposed motor uses rare-earth free ferrite permanent magnets and shows a high torque, low torque ripple, and low induced voltage in electric truck applications.

## II. APPROACH AND RESULTS

### A. Rotor Topology

We have simulated four-rotor topology types with three-phase winding using ANSYS Maxwell 2D-finite element analysis (FEA) v.18.1 to determine the best topology. All motors have 12 slots with conventional three-phase windings and 10 ferrite PMs. Fig. 2 shows the simulated rotor topologies: PM-assisted synchronous reluctance machine (PMASynRM), V-type PMSM, surface-mounted PMSM (SPM), and spoke-type PMSM. Table II summarizes the performance of the simulated rotor topologies. The simulation results show that the spoke-type topology shows the highest torque, good torque ripple, and back EMF at 3000 rpm among the topologies. Therefore, the spoke-type topology is chosen for further performance investigation.

### B. Stator Topology

The multiphase machine recently received much attention due to its fault-tolerance capability and low induced voltage compared with a conventional three-phase machine [5]. Among multiphase machines, the six-phase machine shows the most cost-effective performance because it utilizes two commonly used three-phase inverters in EV application. Therefore, we designed a six-phase ferrite spoke-type PMSM (FSPMSM) and

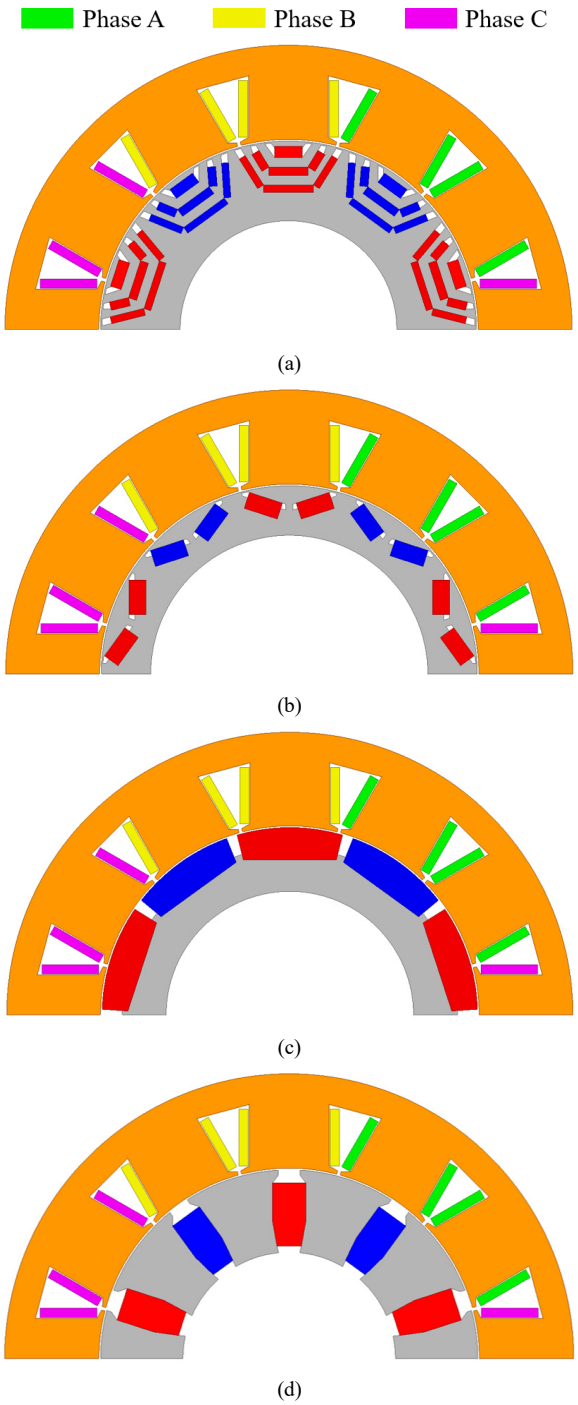


Fig. 2. Design of three-phase FSCW: (a) PMASynRM, (b) V-type, (c) SPM, and (d) spoke-type PMSM.

compared it with a three-phase FSPMSM for motor performance. Fig. 3 illustrates the three- and six-phase FSPMSM. Their performance is compared in Table III. The six-phase FSPMSM exhibits slightly higher torque, 22.1 % lower torque ripple, and 45.1 % lower peak back-EMF at 3000 rpm. However, the torque ripple and peak back-EMF are still too high for use in electric trucks.

Thus, to further reduce the torque ripple and peak back-EMF and increase the maximum torque, we adopted a stator shifting

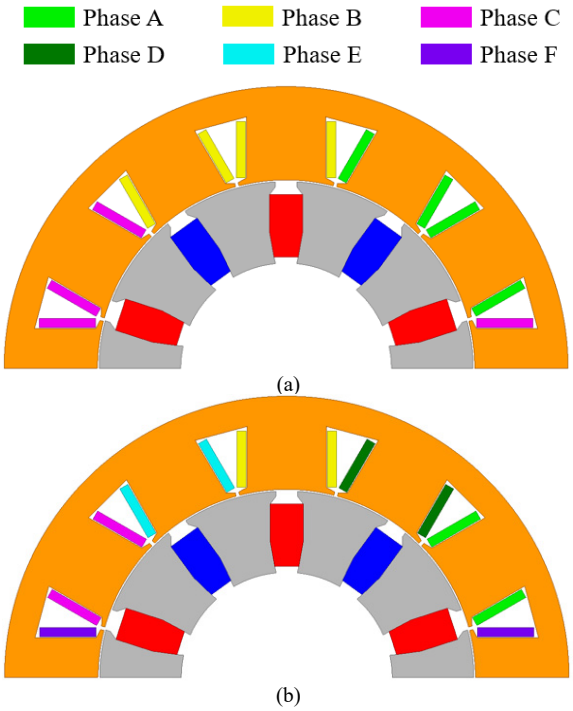


Fig. 3. Design of (a) three-phase and (b) six-phase FSCW ferrite spoke-type motor.

TABLE III. PERFORMANCE COMPARISON BETWEEN THREE- AND SIX-PHASE FSCW FERRITE SPOKE-TYPE MOTOR.

| Parameter | Three-phase | Six-phase |
|---|---|---|
| Torque [Nm] | 1880 | 1920 |
| Torque Ripple [%] | 12.2 | 9.5 |
| Peak Back EMF at 3000 rpm [V] | 2428 | 1320 |

technique within the machine [5]. The stator-shifted machine has an asymmetrical six-phase winding with α of 75 degrees between the two three-phase windings and uses 24 slots, instead of 12 slots, to realize the stator-shifting technique. The primary role of the stator-shift is to reduce the 7th harmonic. Assuming the angle α between the two three-phase winding is limited to 2(k-1)360°/Q, where k is a positive integer and Q is the number of slots, and the magnitude of the 7th harmonic is $F_7$, the sum of the 7th harmonic ($F_{sum}$) of the two three-phase set can be written as

$$\begin{aligned} F_{sum} &= F_7\cos 7\theta + F_7\cos 7(\theta-\alpha) \\ &= F_7\cos 7\theta + F_7\cos 7\left(\theta-(2k-1)15^o\right) \\ &= 2F_7\cos\left(\frac{7\theta+7\left(\theta-(2k-1)15^o\right)}{2}\right)\cos\left(\frac{7\theta-7\left(\theta-(2k-1)15^o\right)}{2}\right) \\ &= 2\cos\left((2k-1)52.5^o\right)\cos\left(7\theta-(2k-1)52.5^o\right) \end{aligned} \quad (1)$$

The 7th harmonic magnitude is minimum when the cos((2k-1)52.5°) is minimum. The minimum occurs when the k is 3 or 10. If k is 3 or 10, then α is 75 or 285°. Fig. 4 shows the conventional 12-slot and 10-pole and stator shifted 24-slot and 10-pole six-phase FSCW FSPMSM. Table IV summarizes the corresponding performance. The number of turns decrease from 64 to 32 as the number of slots increases from 12 to 24 due to reduced slot size. The results show that the stator-shifted 24-slot design's torque is increased by 11.5 %, due to a 65 % decrease in the 7th harmonic. As a result, the torque ripple and induced voltage are decreased by 34.7 and 43.8%, respectively.

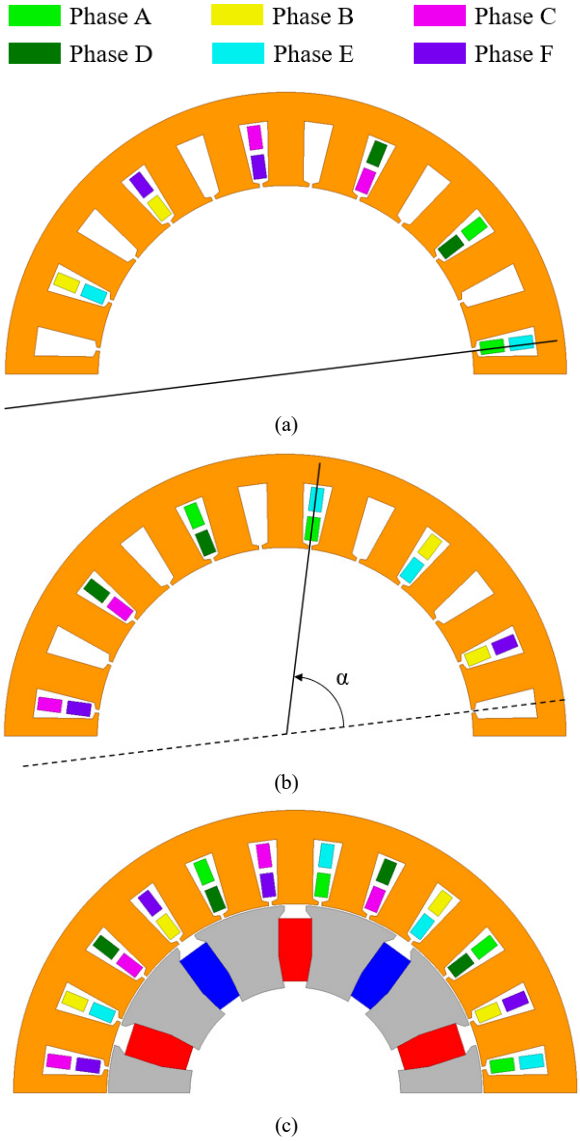


Fig. 4. Design of (a) first and (b) second-set of the 12-slot/10-pole winding layout and (c) resultant 24-slot/10-pole winding layout.

### C. Torque Ripple Reducing Voids

In 2011, the US Department of Energy (DOE) announced the target torque ripple of electrical traction motor to be less than 5 % [6]. To further reduce the torque ripple of 6.2 % to below 5 %, we introduced one circular hole on the stator and one circular notch on the rotor with a diameter of 10 mm, as shown in Fig. 5. A nonmagnetic shaft with a rectangular holder is used to hold the rotor in one piece and rotate it. Table V shows the

TABLE IV. PERFORMANCE COMPARISON BETWEEN UNCONVENTIONAL AND STATOR-SHIFTED 6-S-FSCW-FPMSM.

| Parameter | Conventional 12-slot | Stator-shifted 24-slot |
|---|---|---|
| Number of turns | 64 | 32 |
| Torque [Nm] | 1920 | 2142 |
| Torque Ripple [%] | 9.5 | 6.2 |
| Peak Back EMF at 3000 rpm [V] | 1320 | 742 |
| Normalized 7th Back EMF Harmonic [V] | 0.0465 | 0.0236 |

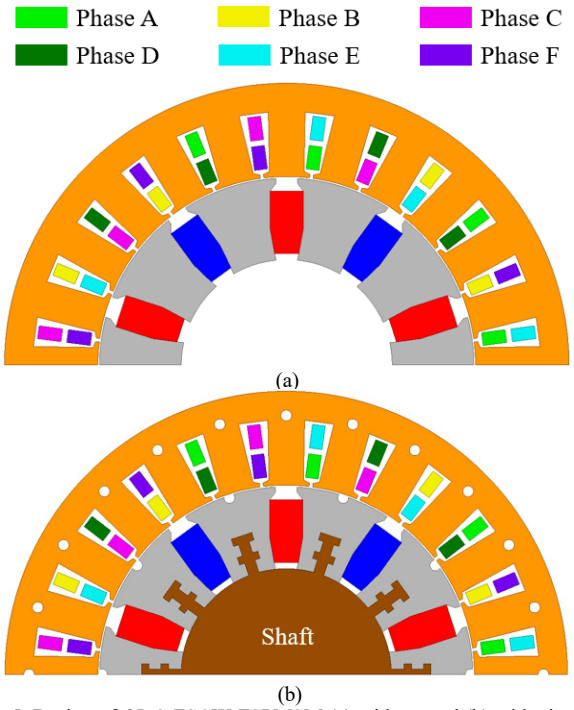


Fig. 5. Design of 6Φ-S-FSCW-FSPMSM (a) without and (b) with circular hole and notch and rectangular nonmagnetic shaft fixture.

TABLE V. PERFORMANCE COMPARISON OF 6Φ-S-FSCW-FSPMSM WITHOUT AND WITH CIRCULAR HOLE AND NOTCH AND SHAFT.

| Parameter | No hole or notch | Hole on stator | Notch on rotor | Hole and Notch | Hole and notch with shaft |
|---|---|---|---|---|---|
| Torque [Nm] | 2142 | 2140 | 2155 | 2150 | 2150 |
| Torque ripple [%] | 6.2 | 5.5 | 4.8 | 4.1 | 4.1 |
| Torque ripple difference from no circular void [%] | - | 11.3 | 22.6 | 33.9 | 33.9 |

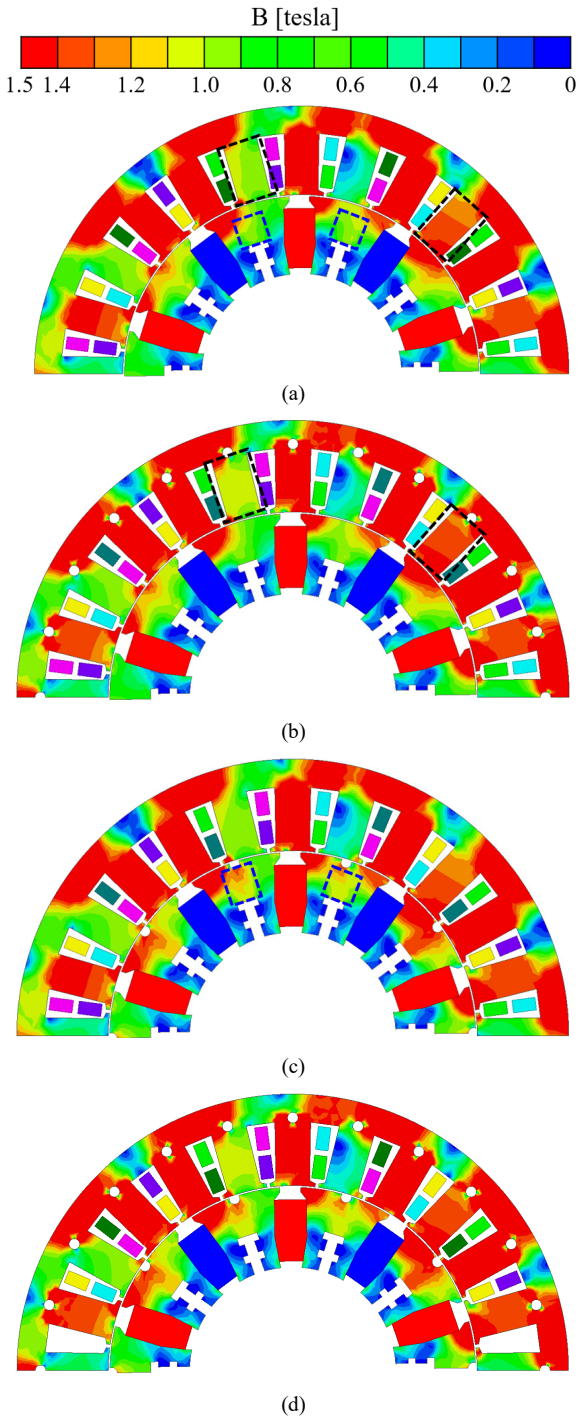


Fig. 6. Flux density distribution of 6Φ-S-FSCW-FSPMSM with (a) shaft only, (b) shaft and circular hole on the stator, (c) shaft and circular notch on the rotor, and (d) shaft, circular hole on the stator, and circular notch on the rotor.

performance of 6Φ-S-FSCW-FSPMSM with and without the circular hole and notch and a rectangular cavity-based nonmagnetic shaft. It was found that the inclusion of the circular hole and notch and nonmagnetic shaft did not alter the peak induced voltage. However, the introduction of the hole and notch significantly decreases the torque ripple of 6Φ-S-FSCW-FSPMSM. When one circular hole is introduced on the stator, the torque ripple was decreased by 11.3 %. This reduction is mainly attributed to the increased flux density between the slots as shown in black dashed rectangular region in Fig. 6 (b). Fig. 6 shows the flux density distribution of the proposed motor without and with hole and notch on the stator and rotor, respectively. Compared to the flux density in the black dashed rectangular region in Fig. 6 (a), the flux density in the black dashed rectangular region in Fig. 6 (b) shows 0.1-0.2 T higher

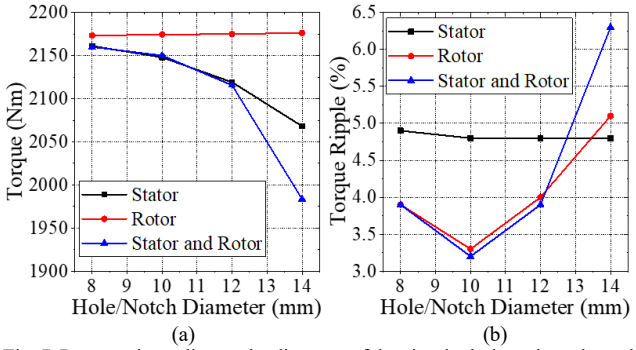


Fig. 7. Parametric studies on the diameter of the circular hole and notch used in the stator, rotor, and both stator and rotor for (a) torque and (b) torque ripple.

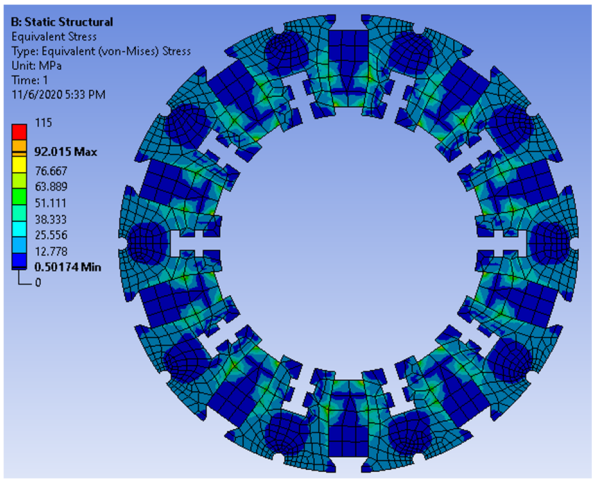


Fig. 8. Mechanical analysis of the proposed 6Φ-S-FSCW-FSPMSM.

values. Further, when the notch is introduced on the edge of the rotor between the PMs, the torque ripple reduction of 22.6 % was achieved. This is mainly due to the increased flux density in blue dashed rectangular region in Fig. 6(c). Compared to the flux density in the blue dashed rectangular region in Fig. 6(a), 0.3-0.4 T higher flux density was observed in the blue dashed rectangular region in Fig. 6(c), resulting 10.8% reduction in total harmonic distortion (THD). By combining these effects, a total of 33.9 % torque ripple reduction was achieved by introducing the hole and notch on the stator and rotor, respectively, without decreasing the peak torque.

A parametric study is conducted on the diameter of the circular hole and notch used in the stator, rotor, and both stator and rotor to observe the effects on the torque and torque ripple. Fig. 7 shows the torque and torque ripple performance of the proposed 6Φ-S-FSCW- FSPMSM for various diameter sizes of the circular hole and notch used in the stator and rotor. As Fig. 7(a) illustrates, the torque remains constant with respect to the increased diameter of the circular notch in the rotor. On the other hand, the torque decreases as the diameter of the circular hole used in the stator increased from 8 to 14 mm. Similarly, the torque of the proposed motor having both circular hole and notch decreases to 1985 Nm. On the contrary, the torque ripple remains constant with respect to the increased diameter of the circular hole in the stator unlike the torque performance. However, the torque ripple of the motor having the circular notch on the rotor and both the circular hole and notch in the

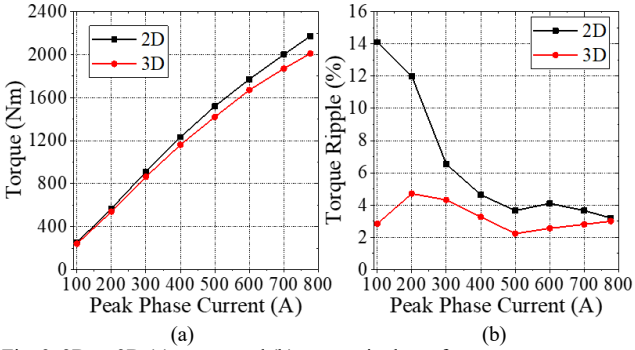


Fig. 9. 2D vs 3D (a) torque and (b) torque ripple performance.

stator and rotor shows a positive quadratic trend. As a result, the lowest torque ripple of 3.21 % was observed for the motor having both circular hole and notch when the diameter reaches 10 mm.

### *D. Mechanical Analysis*

A mechanical FEA analysis was conducted to validate the mechanical stability of the motor by using ANSYS Mechanical. Fig. 8 shows the stress distribution in the rotor of the proposed 6Φ-S-FSCW- FSPMSM at 4500 rpm. The results show that the stress is well below the rotor's stress limit of 345 MPa.

### *E. Irreversible Demagnetization Analysis*

The main drawback of the ferrite PM is low coercivity, which may cause the irreversible demagnetization of the PM from its initial magnetization direction. Thus, the irreversible demagnetization of the ferrite PM is evaluated by observing the rate of irreversible demagnetization (α). The α is calculated by

$$\alpha = A_{irrev\_demag} / A_{tot\_mag} \quad (2)$$

where $A_{irrev\_demag}$ denotes the area where the flux density is below 0.1 T and the $A_{tot\_mag}$ is the total PM area. It is noted that a flux density above 0.1 T is recommended for PMs to prevent the irreversible demagnetization of the PMs [8]. The simulation result shows that the $\alpha$ exceeds 0 when the input current is higher than 3 times of the maximum RMS current of 500 $A_{rms}$.

### *F. 3D-FEA Result*

The proposed motor was further evaluated using ANSYS Maxwell 3D-FEA software to emulate the motor performance in real environment. Fig. 9 shows the maximum torque and torque ripple performance as a function of the peak phase current from 100 to 777 A. As shown in Fig. 9 (a), the maximum torque obtained using 3D-FEA is well matched with that of the 2D-FEA with only 6.5 % lower torque. This torque reduction is mainly attributed to the end effect of the motor. As for the torque ripple, the motor simulated using 3D-FEA showed low torque ripple of 4.7 % for all input current, satisfying the US DOE target torque ripple of 5 %.

### *G. Performance Comparison between Prius and Proposed Motor*

Lastly, the proposed motor design with the hole, notch, and the shaft is compared with conventional three-phase ISDW V-type PMSM used in Toyota Prius with Nd-Fe-B and ferrite [7],

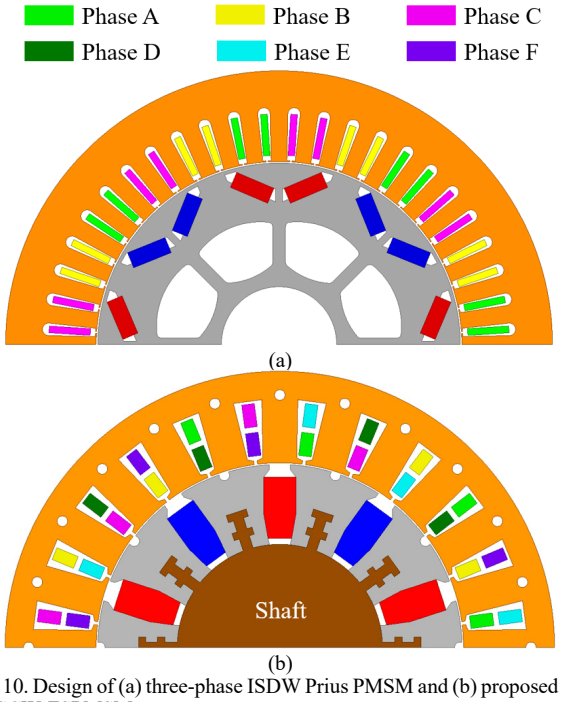


Fig. 10. Design of (a) three-phase ISDW Prius PMSM and (b) proposed 6Φ-S-FSCW-FSPMSM.

TABLE VI. PERFORMANCE COMPARISON BETWEEN PRIUS MOTOR WITH NDFEB AND FERRITE AND PROPOSED MOTOR.

| **Parameter** | **Prius (NdFeB)** | **Prius (Ferrite)** | **Proposed motor (Ferrite)** |
|---|---|---|---|
| Peak torque [Nm] | 2133.4 | 2180 | 2150 |
| Torque ripple [%] | 22.6 | 19.8 | 4.1 |
| Back EMF at 3000 rpm [V] | 2500 | 3790 | 740 |
| Volume [L] | 43.3 | 60.6 | 58.4 |
| Peak torque density [Nm/L] | 49.3 | 35.9 | 37.0 |
| Demagnetization [%] | 0 | 10 | 0 |
| Battery Voltage [V] | | 700 | |
| Base speed [rpm] | 750 | 450 | 2400 |
| Maximum speed [rpm] | 1750 | 950 | 4950 |

as illustrated in Fig. 10, to assess the proposed 6Φ-S-FSCW-FSPMSM performance. Table VI shows the performance comparison between the Prius motor with NdFeB and ferrite and the proposed motor. The proposed 6Φ-S-FSCW-FSPMSM exhibits comparable peak torque, 131.4 – 138.6 % lower torque ripple, 108.6 – 134.6 % lower induced voltage at 3000 rpm, -3 – 28.5 % lower peak torque density, no demagnetization, and 95.5 – 135.6 % higher maximum speed compared to the Prius motor with NdFeB and ferrite.

## III. CONCLUSION

The proposed 6Φ-S-FSCW-FSPMSM employs stator-shifted dual three-phase fractional slot concentrated windings that are 75 degrees apart between two three-phase windings and a spoke-type rotor topology using cost-effective and highly resistant ferrite. The proposed 6Φ-S-FSCW-FSPMSM can drive electric trucks with a good peak torque of 2150 Nm, low peak torque ripple of 3.2 %, and high maximum speed of 4950 rpm.

## REFERENCES

[1] MarketsandMarkets, Electric Vehicle Market by Vehicle (Passenger Cars & Commercial Vehicles), Vehicle Class (Mid-priced & Luxury)…. Online: https://www.marketsandmarkets.com/Market-Reports/electric-vehicle-market-209371461.html.

[2] BEnvironmental leaders, "Electric Drive Truck Sales by Powertrain Type, World Markets: 2016-2026," Navigant Research. Online: https://www.environmentalleader.com/wp-content/uploads/2017/01/Navigant-Research-electric-truck-forecast.jpg.

[3] D. Smith, et al., "Medium- and Heavy-duty Vehicle Electrification An Assessment of Technology and Knowledge Gap," ORNL/SPR-2020/7, Dec. 2019.

[4] E. Hernandez, "Nissan LEAF electric motor and transmission," Living LEAF, Nov. 2010, [URL: http://livingleaf.info/2010/11/nissan-leaf-electric-motor-and-transmission/].

[5] L. Cheng, Y. Sui, P. Zheng, Z. Yin and C. Wang, "Influence of Stator MMF Harmonics on the Utilization of Reluctance Torque in Six-phase PMASynRM with FSCW," *Energies* **11**, 108, pp. 1-17, Oct. 2017.

[6] A. El-Refaie, J. P. Alexander, S. Galioto, P. B. Reddy, K. Huh, P. Bock, and X. Shen, "Advanced High-Power-Density Interior Permanent Magnet Motor for Traction Applications," *IEEE Transactions on Industry Application* **50**, 1, pp. 3235-3248, Sept/Oct. 2014.

[7] M. Olszewski, "Evaluation of the 2010 Toyota Prius Hybrid Synergy Drive System," *FY2011 Oak Ride National Laboratory Report*, Mar. 2011.

[8] H. Won, Y. Hong, W. Lee, and M. Choi, "Roles of coercivity and remanent flux density of permanent magnet in interior permanent magnet synchronous motor (IPMSM) performance for electric vehicle applications," *AIP Advances*, **8**, pp. 056811, Jan. 2018.